

1           Impacts of the East Asian summer monsoon on interannual variations of  
2                           summertime surface-layer ozone concentrations over China

3  
4  
5

6                           Yang Yang<sup>a,b</sup>, Hong Liao<sup>a,\*</sup>, and Jianping Li<sup>c</sup>

7

8   <sup>a</sup>State Key Laboratory of Atmospheric Boundary Layer Physics and Atmospheric  
9    Chemistry, Institute of Atmospheric Physics, Chinese Academy of Sciences, Beijing,  
10   China.

11   <sup>b</sup>Graduate University of Chinese Academy of Science, Beijing, China.

12   <sup>c</sup>State Key Laboratory of Numerical Modeling for Atmospheric Sciences and Geophysical  
13    Fluid Dynamics, Institute of Atmospheric Physics, Chinese Academy of Sciences,  
14    Beijing, China.

15

16

17

18

19   \*Corresponding author address:

20   Prof. Hong Liao  
21   LAPC, Institute of Atmospheric Physics  
22   Chinese Academy of Sciences  
23   Beijing 100029, China  
24   E-mail: [hongliao@mail.iap.ac.cn](mailto:hongliao@mail.iap.ac.cn)

25 **Abstract**

26 We apply a global three-dimensional Goddard Earth Observing System  
27 (GEOS) chemical transport model (GEOS-Chem) driven by the NASA/GEOS-4  
28 assimilated meteorological fields to quantify the impacts of the East Asian  
29 summer monsoon (EASM) on interannual variations of June-July-August (JJA)  
30 surface-layer O<sub>3</sub> concentrations over China. With anthropogenic emissions fixed  
31 at year 2005 levels, model simulation for years 1986–2006 shows that the  
32 changes in meteorological parameters alone lead to interannual variations in JJA  
33 surface-layer O<sub>3</sub> concentrations by 2–5% over central eastern China, 1–3% in  
34 northwestern China, and 5–10% over the Tibetan Plateau as well as the border  
35 and coastal areas of South China, as the interannual variations are relative to the  
36 average O<sub>3</sub> concentrations over the 21-yr period. Over 1986–2006, O<sub>3</sub>  
37 concentration averaged over the whole China is found to correlate positively with  
38 the EASM index with a large correlation coefficient of +0.75, indicating that JJA O<sub>3</sub>  
39 concentrations are lower (or higher) in weaker (or stronger) EASM years. Relative  
40 to JJA surface-layer O<sub>3</sub> concentrations in the strongest EASM years (1990, 1994,  
41 1997, 2002, and 2006), O<sub>3</sub> levels in the weakest EASM years (1988, 1989, 1996,  
42 1998, and 2003) are lower over almost whole China with a national mean lower  
43 O<sub>3</sub> concentration by 2.0 ppbv (or 4%). Regionally, the largest percentage  
44 differences in O<sub>3</sub> concentration between the weakest and strongest EASM years  
45 are found to exceed 6% in northeastern China, southwestern China, and over the

46 Tibetan Plateau. Sensitivity studies show that the difference in transboundary  
47 transport of O<sub>3</sub> is the most dominant factor that leads to lower O<sub>3</sub> concentrations  
48 in the weakest EASM years than in the strongest EASM years, which, together  
49 with the enhanced vertical convections in the weakest EASM years, explain about  
50 80% of the differences in surface-layer O<sub>3</sub> concentrations between the weakest  
51 and strongest EASM years. We also find that the impacts the EASM strength on  
52 JJA surface-layer O<sub>3</sub> can be particularly strong (comparable in magnitude to the  
53 impacts on O<sub>3</sub> by changes in anthropogenic emissions over 1986–2006) for  
54 certain years. The largest increases in O<sub>3</sub> by anthropogenic emissions are  
55 simulated over southeastern China, whereas the largest impacts of the EASM on  
56 O<sub>3</sub> are found over central and western China.

57 **1 Introduction**

58 Tropospheric O<sub>3</sub> is an air pollutant harmful to human health and ecosystems  
59 (Shindell et al., 2012). It is also (after CO<sub>2</sub> and CH<sub>4</sub>) the third most important  
60 anthropogenic greenhouse gas (Intergovernmental Panel on Climate Change  
61 (IPCC), 2007). High O<sub>3</sub> concentrations have been observed in many Chinese  
62 sites, with seasonal mean concentrations of 20–60 ppbv (Tang et al., 1995; Yan  
63 et al., 1997, 2003; Cheung and Wang, 2001; Zhu et al., 2004; Gao et al., 2005;  
64 Shao et al., 2006; H. Wang et al., 2005; Chou et al., 2006; Ding and Wang, 2006;  
65 T. Wang et al., 2006a, 2009; Takami et al., 2006; Tu et al., 2007; Ding et al., 2008;  
66 Lin et al., 2008; Xu et al., 2008; Yang et al., 2008; Zhang et al., 2008; Y. Wang et  
67 al., 2011) and episodic concentrations of exceeding 100 ppbv (T. Wang et al.,  
68 2006b; Z. Wang et al., 2006; Duan et al., 2008). Concentrations of O<sub>3</sub> are driven  
69 by a combination of precursor emissions and the regional meteorological  
70 conditions.

71 Meteorological parameters in summer in eastern China vary with the East  
72 Asian summer monsoon (EASM). The EASM prevails in May–September every  
73 year, with strong southerlies bringing clean, warm, and moist air from the oceans  
74 to eastern China and rain belts that stretch for thousands of kilometers in the  
75 west–east direction in eastern China (Tao and Chen, 1987; Wang and Ding,  
76 2008). Previous observational and modeling studies have shown that such  
77 patterns of winds and precipitation of the EASM influence the seasonal variations

78 of O<sub>3</sub> in China (Chan et al., 1998; Li et al., 2007; He et al., 2008; Wang et al., 2011)  
79 and in the west Pacific region (Pochanart et al., 2002; Tanimoto et al., 2005;  
80 Yamaji et al., 2006). He et al. (2008) analyzed the seasonal variations of O<sub>3</sub>  
81 concentrations measured over 2004–2006 and found that O<sub>3</sub> concentrations peak  
82 in spring and autumn with a summer trough in central eastern China and the west  
83 Pacific, the areas that are influenced by clean air from the southern oceans during  
84 the summer monsoon. Studies by Wang et al. (2008), Lin et al. (2009), and Zhao  
85 et al. (2010) reported that the increasing clouds associated with the EASM rainfall  
86 suppress photochemical production of O<sub>3</sub> by altering solar radiation, which also  
87 contribute to the minimum O<sub>3</sub> concentrations in summer.

88       The strength of the EASM exhibits large interannual variations as a result of  
89 the interactions between the atmosphere and oceans (Webster et al., 1998). No  
90 previous studies, to our knowledge, have systematically examined the impacts of  
91 the EASM on interannual variations of summertime O<sub>3</sub> in China. Recently, Zhou et  
92 al. (2013) analyzed 2000–2010 ozonesonde data from Hong Kong and found a  
93 close link between lower tropospheric O<sub>3</sub> and the East Asian monsoon on  
94 interannual scales, but their analyses were focused on O<sub>3</sub> in Hong Kong in spring  
95 and autumn. We present here a study to examine the impacts of the EASM on  
96 interannual variations of summertime surface-layer O<sub>3</sub> concentrations over China,  
97 based on 1986–2006 simulations of O<sub>3</sub> concentrations using the global chemical  
98 transport model GEOS-Chem driven by the assimilated meteorological fields. This

99 work is a companion study to the work of Zhu et al. (2012), which investigated the  
100 impacts of the EASM on interannual to decadal variations of summertime  
101 aerosols in China.

102 The GEOS-Chem model and numerical experiments are described in Sect. 2.  
103 Section 3 presents simulated interannual variations of summertime O<sub>3</sub> in China.  
104 Section 4 shows simulated impacts of the EASM on interannual variations of  
105 summertime O<sub>3</sub>, and Sect. 5 examines the mechanisms through which the EASM  
106 influences the interannual variations. Section 6 compares the impacts of changing  
107 monsoon strength with those of changing anthropogenic emissions on O<sub>3</sub>  
108 concentrations in China.

109

## 110 **2 Model description and experimental design**

### 111 **2.1 GEOS-Chem model**

112 We simulate tropospheric O<sub>3</sub> using the global chemical transport model  
113 GEOS-Chem (version 8.2.1, <http://acmg.seas.harvard.edu/geos>) driven by the  
114 assimilated meteorological fields from the Goddard Earth Observing System  
115 (GEOS) of the NASA Global Modeling and Assimilation Office (GMAO). The  
116 version of the model used here has a horizontal resolution of 2° latitude by 2.5°  
117 longitude and 30 vertical layers from the surface to 0.01 hPa. The GEOS-Chem  
118 model includes a fully coupled treatment of tropospheric O<sub>3</sub>-NO<sub>x</sub>-VOC chemistry  
119 and aerosol components. Tropospheric O<sub>3</sub> is simulated with about 80 species and  
120 over 300 chemical reactions (Bey et al., 2001). Photolysis rates are computed

121 using the Fast-J algorithm (Wild et al., 2000). The cross-tropopause O<sub>3</sub> flux in this  
122 version of GEOS-Chem is specified with the synthetic ozone (“Synoz”) method  
123 (McLinden et al., 2000) as implemented by Bey et al. (2001), which includes a  
124 passive, ozone-like tracer released into the stratosphere at a constant rate  
125 equivalent to that of the prescribed cross-tropopause ozone flux of 499 Tg O<sub>3</sub> yr<sup>-1</sup>.

## 126 **2.2 Emissions**

127 Global emissions of O<sub>3</sub> precursors, aerosol precursors, and aerosols in the  
128 GEOS-Chem model follow Park et al. (2003, 2004), but anthropogenic emissions  
129 of NO<sub>x</sub>, CO, SO<sub>2</sub>, and NH<sub>3</sub> over East Asia are overwritten by the emissions  
130 inventory of Streets et al. (2003). Global anthropogenic emissions of nonmethane  
131 hydrocarbons are from the GEIA inventory (Piccot et al., 1992). Biomass burning  
132 emissions are taken from the GFED-2 inventory (van der Werf et al., 2006). These  
133 inventories are then scaled for 2005 on the basis of economic data and energy  
134 statistics as described by van Donkelaar et al. (2008). The biogenic emissions in  
135 the GEOS-Chem model are simulated using the MEGAN module (Guenther et al.,  
136 2006; Wiedinmyer et al., 2007). Soil NO<sub>x</sub> emissions are computed using a  
137 modified version of the algorithm proposed by Yienger and Levy (1995). Lightning  
138 emissions follow Price and Rind (1992), with the NO<sub>x</sub> vertical profile proposed by  
139 Pickering et al. (1998).

140 The simulations of tropospheric O<sub>3</sub> by the GEOS-Chem model have been  
141 evaluated in previous studies for the United States (Fiore et al., 2005; Wu et al.,  
142 2008; H. Wang et al., 2009) and China (Y. Wang et al., 2008, 2011; Jeong and

143 Park, 2013; Lou et al., 2014). The model was found to be able to capture the  
144 magnitude and spatial distribution of O<sub>3</sub> in China.

### 145 **2.3 Experiments**

146 In this study concentrations of O<sub>3</sub> in China for years 1986–2006 are simulated  
147 using the GEOS-4 meteorological fields. To identify the key processes that  
148 influence O<sub>3</sub> concentrations in different monsoon years, we perform the following  
149 simulations:

150 (1) O3\_TOT: The standard simulation of O<sub>3</sub> concentrations for years 1986–2006.

151 Global anthropogenic and biomass burning emissions of NO<sub>x</sub>, CO,  
152 nonmethane hydrocarbons, aerosols and aerosol precursors are fixed at year  
153 2005 levels. Meteorological fields are allowed to vary over 1986–2006. The  
154 cross-tropopause O<sub>3</sub> flux is set to 499 Tg yr<sup>-1</sup> using the “Synoz” scheme.

155 (2) O3\_TB: The sensitivity simulation of O<sub>3</sub> concentrations for years 1986–2006  
156 to quantify the role of transboundary transport of O<sub>3</sub> in different monsoon  
157 years. The model setups are the same as those in O3\_TOT except that all  
158 natural and anthropogenic emissions in China are turned off.

159 (3) O3\_ST: The sensitivity simulation of O<sub>3</sub> concentrations for years 1986–2006  
160 to quantify the impact of cross-tropopause O<sub>3</sub> flux on surface-layer O<sub>3</sub>  
161 concentrations. The model setups are the same as those in O3\_TOT except  
162 that natural and anthropogenic emissions are turned off globally.

163 (4) O3\_EMIS: The sensitivity simulations to compare the impacts of changing

164 anthropogenic emissions with those of changing monsoon strength. Two  
165 sensitivity simulations are conducted with 1986 and 2006 anthropogenic  
166 emissions, respectively. The emissions in year 1986 are simulated using the  
167 default scaling factors in the model (van Donkelaar et al., 2008). Year 2006  
168 meteorological parameters are used to drive both simulations. The  
169 cross-tropopause O<sub>3</sub> flux is set to 499 Tg yr<sup>-1</sup> using the “Synoz” scheme.

#### 170 **2.4 East Asian summer monsoon index**

171 The interannual variations in strength of the EASM are commonly represented by  
172 the EASM index (EASMI). The EASMI introduced by Li and Zeng (2002) is used in  
173 this study. The formulation for calculating EASMI based on the GEOS-4  
174 meteorological parameters was given in Zhu et al. (2012). Positive values of  
175 EASMI indicate strong monsoon years whereas negative values indicate weak  
176 monsoon years. Physically, a strong summer monsoon in China is characterized  
177 by strong southerlies extending from southern China to northern China, a deficit of  
178 rainfall in the middle and lower reaches of the Yangtze River, and large rainfall in  
179 northern China. On the contrary, in a weak summer monsoon year, China  
180 experiences weak southerlies, large rainfall in southern China, and a deficit of  
181 rainfall in northern China. The movement of the rain belts is associated with the  
182 strength of the southerlies.

183

### 184 **3 Simulated interannual variations of summertime O<sub>3</sub> in China**

185 Figure 1a shows the simulated spatial distribution of June-July-August (JJA)  
186 surface-layer O<sub>3</sub> concentrations averaged over 1986–2006 from the O<sub>3</sub>\_TOT  
187 simulation. Over eastern China, simulated O<sub>3</sub> concentrations are 50–65 ppbv in  
188 northern China and 25–50 ppbv in southern China. Such pattern of higher O<sub>3</sub>  
189 concentrations in northern China than in southern China results from that the  
190 strong southerlies bring clean air from the oceans to southern China during the  
191 summer monsoon season (Chan et al., 1998; Yamaji et al., 2006; Li et al., 2007;  
192 He et al., 2008; Wang et al., 2011). In western China, simulated O<sub>3</sub> exhibits  
193 maximum concentrations of 65 ppbv. Our simulated surface-layer concentrations  
194 of O<sub>3</sub> are high in both western and eastern China, which agree with the modeling  
195 studies of Wang et al. (2011), Jeong and Park (2013), and Lou et al. (2014). The  
196 high O<sub>3</sub> concentrations in western China are associated with the downward  
197 transport of O<sub>3</sub> from the stratosphere to troposphere (Wild and Akimoto, 2001; T.  
198 Wang et al. 2006a; Ding and Wang, 2006), and the high O<sub>3</sub> concentrations in  
199 eastern China result from anthropogenic emissions (Wang et al., 2011).

200 The interannual variations in simulated JJA O<sub>3</sub> concentrations can be  
201 quantified by mean absolute deviation (MAD) and absolute percent departure  
202 from the mean (APDM) defined as  $MAD = \frac{1}{n} \sum_{i=1}^n \left| P_i - \frac{1}{n} \sum_{i=1}^n P_i \right|$  and  $APDM =$   
203  $100\% \times MAD / \left( \frac{1}{n} \sum_{i=1}^n P_i \right)$ , where  $P_i$  is the simulated JJA mean O<sub>3</sub> concentration of  
204 year  $i$ , and  $n$  is the number of years examined ( $n=21$  for years 1986–2006).  
205 Therefore MAD represents the absolute interannual variation and APDM

206 represents the interannual variation relative to the average of O<sub>3</sub> concentration  
207 over the  $n$  years. The MAD values of JJA surface-layer O<sub>3</sub> concentrations (Fig.  
208 1b) are 1.0–4.0 ppbv in China, with the largest values exceeding 2 ppbv found  
209 over northeastern China, coastal areas of South China, and the Tibetan Plateau.  
210 As shown in Fig. 1c, the APDM values are in the range of 2–5% over central  
211 eastern China where summer monsoon prevails, 1–3% in northwestern China,  
212 and 5–10% over the Tibetan Plateau as well as the border and coastal areas of  
213 South China. These interannual variations in O<sub>3</sub> are significant as compared to  
214 the impacts of reductions in emissions of O<sub>3</sub> precursors. Han et al. (2005) showed  
215 by modeling studies that, in eastern China, reductions in NO<sub>x</sub> or total VOCs  
216 (anthropogenic plus biogenic VOCs) by 50% lead to changes in JJA O<sub>3</sub>  
217 concentrations by 10–20%.

218 The GEOS-Chem simulations of present-day surface-layer O<sub>3</sub> concentrations  
219 in China have been evaluated in Wang et al. (2011) and Lou et al. (2014). Wang  
220 et al. (2011) demonstrated that the model captured well the magnitude and  
221 seasonal variation of surface-layer concentrations and column burdens of O<sub>3</sub> in  
222 China. Lou et al. (2014) reported that the simulated O<sub>3</sub> in China agreed fairly well  
223 with measurements collected from the literature with an average high bias of 9%.  
224 Because of the lack of long-term O<sub>3</sub> measurements in China, we evaluate the  
225 simulated interannual variations of JJA surface-layer O<sub>3</sub> concentrations at two  
226 sites (Fig. 2): Hok Tsui in Hong Kong (22°13' N, 114°15' E) and Ryori in Japan

227 (39°03'N, 144°82'E). The measurements at Hok Tsui are taken from T. Wang et al.  
228 (2009), and those at Ryori site are from the WMO World Data Center for  
229 Greenhouse Gases (WDCGG, <http://ds.data.jma.go.jp/gmd/wdcgg/>). At Hok  
230 Tsui, simulated O<sub>3</sub> concentrations are higher than the observations in JJA. This  
231 discrepancy may due to the model's overestimate of O<sub>3</sub> in marine boundary layers  
232 in summer (Liu et al., 2006). Interannually, the model captures well the peaks and  
233 troughs of the observed JJA O<sub>3</sub> concentrations, with a high correlation coefficient  
234 of +0.87. The model underestimates JJA O<sub>3</sub> concentrations at Ryori, probably due  
235 to the uncertainties with local emissions, but captures mostly the years with  
236 maximum or minimum O<sub>3</sub> levels with a correlation coefficient of +0.47. The  
237 simulated APDM values at Hok Tsui and Ryori are both 7%, smaller than the  
238 observed interannual variations of 22% and 8% at these two sites, respectively,  
239 which can be attributed to the fixed anthropogenic emissions of O<sub>3</sub> precursors in  
240 our O<sub>3</sub>\_TOT simulation.

241

#### 242 **4 Impacts of the EASM on interannual variations of summertime O<sub>3</sub> in** 243 **China**

244 Simulated JJA surface-layer O<sub>3</sub> concentration averaged over the whole China  
245 (defined by the national borders of China) is shown in Fig. 3a for years 1986–2006  
246 based on the O<sub>3</sub>\_TOT simulation. Summertime O<sub>3</sub> concentrations show large  
247 interannual variations, with high (or low) O<sub>3</sub> concentrations in strong (or weak)

248 monsoon years. Concentrations of O<sub>3</sub> are found to correlate positively with the  
249 EASMI; the correlation coefficient is +0.75 and is statistically significant at the  
250 95th percentile. The spatial distribution of the correlation coefficients between the  
251 EASMI and O<sub>3</sub> concentrations from the O<sub>3</sub>\_TOT simulation is presented in Fig. 3b.  
252 Positive correlations are found in almost the whole China, and large positive  
253 correlation coefficients that exceed +0.5 are found over the region between 90°E  
254 and 110°E. Since anthropogenic emissions of O<sub>3</sub> precursors are kept unchanged  
255 in the simulation for 1986–2006, these strong positive correlations demonstrate  
256 that the EASM strength has large impacts on JJA O<sub>3</sub> concentrations over China.

257 In order to quantify the impacts of the EASM on O<sub>3</sub> concentrations over China,  
258 we show in Figs. 4a and 4b, respectively, the absolute and percentage differences  
259 between O<sub>3</sub> concentrations averaged over five weakest EASM years (1988, 1989,  
260 1996, 1998, and 2003) and those averaged over five strongest EASM years (1990,  
261 1994, 1997, 2002, and 2006). These weakest (or strongest) monsoon years are  
262 selected within 1986–2006 based on the five largest negative (or positive) values  
263 of the normalized EASMI as shown in Fig. 3a. Relative to the concentrations in the  
264 strongest monsoon years, O<sub>3</sub> levels in the weakest monsoon years are lower over  
265 almost the whole China, with the largest reductions of exceeding 3 ppbv (or 6%) in  
266 northeastern and southwestern China and over or near the Tibetan Plateau.  
267 Concentrations of O<sub>3</sub> in the weakest monsoon years are simulated to be higher  
268 than those in the strongest monsoon years by 3–5 ppbv (or 6–15%) over the East

269 China Sea. The pattern of the differences in  $O_3$  concentrations agrees with the  
270 spatial distribution of the correlation coefficients (Fig. 3b). Averaged over China,  
271  $O_3$  level in the weakest monsoon years is lower than that in the strongest  
272 monsoon years by 2.0 ppbv (or 4%). Note that the monsoon region covers almost  
273 the whole China except for the northwestern China (Gao, 1962; An et al., 2000).  
274 Our simulated monsoon-induced changes in  $O_3$  in China (Fig. 4) are mostly within  
275 the monsoon region. The changes in  $O_3$  over the Siberia are large, which can be  
276 explained by the anomalous northerlies over the north border of China between  
277 the five weakest and strongest EASM years (weakest–strongest) (Fig. 5) that  
278 transport  $O_3$  to China.

279 Figures 4c and 4d are pressure-longitude plots of the differences in  $O_3$   
280 averaged over the latitude range of  $20^\circ$ – $46^\circ$ N. From the surface to 250 hPa  
281 altitude,  $O_3$  levels in the weakest monsoon years are lower by up to 5 ppbv (or 8%)  
282 over  $80^\circ$ – $115^\circ$ E and are higher by 1–3 ppbv (or 3–6%) over  $120^\circ$ – $135^\circ$ E relative  
283 to the concentrations in the strongest monsoon years. Concentrations of  $O_3$  at  
284 130–250 hPa altitudes exhibit increases in the weakest monsoon years, with  
285 maximum increases of 4–7 ppbv (3–6%) over  $80^\circ$ E and  $130^\circ$ E, as a result of the  
286 anomalous horizontal convergence at these layers.

287

## 288 **5 Mechanisms of the impacts of the EASM on summertime $O_3$**

### 289 **5.1 Impacts of the EASM on transboundary transport of $O_3$**

290 Considering that O<sub>3</sub> concentrations in almost whole China are lower in the  
291 weakest monsoon years than in the strongest monsoon years and that  
292 tropospheric O<sub>3</sub> has a relatively long lifetime of 3–4 weeks (Seinfeld and Pandis,  
293 2006), we examine firstly the impacts of the EASM on transboundary transport of  
294 O<sub>3</sub>. Figure 5 shows JJA horizontal winds at 850 hPa and 500 hPa averaged over  
295 1986–2006 as well as the composite differences in JJA horizontal winds between  
296 the five weakest and five strongest EASM years at these two layers. The typical  
297 features in winds during the EASM can be seen in Figs. 5a and 5b. The  
298 southerlies prevail in southeastern China in the lower and middle troposphere in  
299 JJA. Figs. 5c and 5d also present the differences in winds between the weakest  
300 and strongest EASM years (weakest minus strongest). In JJA, anomalous  
301 southerlies are found in southern China and anomalous westerlies are found in  
302 southeastern China, as the winds in the five weakest monsoon years are  
303 compared with those in the five strongest monsoon years. Such differences in  
304 winds between weak and strong EASM years were also reported in Li and Zeng  
305 (2002) and Huang (2004).

306 The differences in winds in different monsoon years lead to differences in  
307 transboundary transport of O<sub>3</sub>. We show in Fig. 6 the differences in simulated  
308 horizontal mass fluxes of O<sub>3</sub> at the four lateral boundaries of the selected box of  
309 (85°–120°E, 20°–46°N, the surface to 250 hPa) and in Table 1 the summary of the  
310 composite analysis on fluxes of O<sub>3</sub> in and out of this box, based on simulation

311 O3\_TOT. This box is selected to capture the features of transboundary O<sub>3</sub>  
312 transport that influence O<sub>3</sub> concentrations in China. The location of the box is  
313 shown in Fig. 5d. Relative to the strongest monsoon years, the weakest monsoon  
314 years have less inflow by 0.1 Tg season<sup>-1</sup> at the west boundary, larger inflow  
315 fluxes of O<sub>3</sub> by 4.2 Tg season<sup>-1</sup> at the south boundary and by 5.5 Tg season<sup>-1</sup> at  
316 the north boundary, and larger outflow by 12.9 Tg season<sup>-1</sup> at the east boundary  
317 (Table 1 and Fig. 6), as mass fluxes are summed over JJA. The net effect is a  
318 larger transboundary outflow of O<sub>3</sub> by 3.3 Tg season<sup>-1</sup> in the weakest monsoon  
319 years than in the strongest monsoon years. The anomalous westerlies in  
320 southeastern China are especially important, which bring polluted air with high O<sub>3</sub>  
321 concentrations to the coastal areas and the East China Sea (Fig. 6d), leading to  
322 reductions in O<sub>3</sub> concentration in China.

323 The role of changes in transboundary transport of O<sub>3</sub> can be further quantified  
324 by the simulation O3\_TB with natural and anthropogenic emissions of O<sub>3</sub>  
325 precursors in China turned off. The spatial distribution of O<sub>3</sub> from simulation  
326 O3\_TB (referred to as TBO<sub>3</sub> hereafter) is presented in Fig. 7a. TBO<sub>3</sub>  
327 concentrations show a distinct spatial gradient over China, decreasing from about  
328 55 ppbv in northwestern China to about 10 ppbv in southeastern China. The JJA  
329 TBO<sub>3</sub> concentration averaged over the whole China is 30 ppbv, which is about 62 %  
330 of the average concentration simulated in O3\_TOT, indicating that a significant  
331 fraction of surface-layer O<sub>3</sub> over China is from transboundary transport. The

332 differences in TBO<sub>3</sub> concentrations between the weakest and strongest monsoon  
333 years (Fig. 7d) are, to a large extent, similar to those from simulation O3\_TOT (Fig.  
334 4a), in terms of both distributions and magnitudes. Averaged over China, the  
335 difference in TBO<sub>3</sub> between the weakest and strongest monsoon years is -1.6  
336 ppbv, which accounts for 80% of the corresponding difference obtained in  
337 O3\_TOT. The JJA mass fluxes of TBO<sub>3</sub> for the selected box of (85°–120°E, 20°–  
338 46°N, the surface to 250hPa) are also similar to those simulated in O3\_TOT  
339 (Table 1), with a net horizontal outflow of 2.8 Tg season<sup>-1</sup>. These model results  
340 indicate that the differences in transboundary transport of O<sub>3</sub> is a dominant  
341 mechanism through which the EASM influences interannual variations of JJA O<sub>3</sub>  
342 concentrations in China.

## 343 **5.2 Impacts of the EASM on vertical transport of O<sub>3</sub>**

344 Vertical circulations in China have some unique features during the EASM. In  
345 summer, two major ascending branches of winds (or strong convections) are  
346 observed throughout the entire troposphere (Fig. 8a). One branch is located over  
347 the Yangtze River valley, associated with the Mei-yu front (rain belt) of the EASM  
348 (Ding and Chan, 2005). The other branch is over the Tibetan Plateau, because  
349 the Tibetan Plateau during summer serves as a large heat source, which uplifts  
350 heated air to the upper troposphere and even to the stratosphere (Ye, 1981). Fig.  
351 8a shows JJA vertical velocity and simulated vertical mass flux of O<sub>3</sub> at 500 hPa  
352 averaged over 1986–2006. Since vertical velocity is not available from the

353 reanalyzed GEOS-4 meteorological fields, vertical winds presented here are from  
354 the NCEP/NACR reanalysis data. The simulated mass fluxes are obtained in  
355 O3\_TOT. The largest vertical mass fluxes of O<sub>3</sub> are simulated to occur over  
356 northern China and western China where surface-layer O<sub>3</sub> concentrations are  
357 high, and to occur over the Tibetan Plateau and its surrounding areas as a result  
358 of the strong convections here.

359 Figure 8b shows the differences in JJA vertical wind velocity and simulated  
360 vertical mass flux of O<sub>3</sub> at 500 hPa between the weakest and strongest monsoon  
361 years. Relative to the strongest monsoon years, anomalous convections are  
362 found over central and western China in the weakest monsoon years, leading to  
363 enhanced upward transport of O<sub>3</sub> from the surface to upper troposphere at these  
364 locations. The differences in vertical winds shown in Fig. 8b agree with those  
365 reported in Huang (2004).

366 Table 1 also summarizes the composite analysis on vertical fluxes of O<sub>3</sub>  
367 through the top side of the selected box (85°–120°E, 20°–46°N, the surface to  
368 250hPa). In simulation O3\_TOT, the upward flux of O<sub>3</sub> through the top plane of  
369 the box in the weakest monsoon years is larger than that in the strongest  
370 monsoon years by 1.4 Tg season<sup>-1</sup>. This anomalous vertical outflow of 1.4 Tg  
371 season<sup>-1</sup> is smaller than the anomalous horizontal transboundary outflow of 3.3  
372 Tg season<sup>-1</sup> (Section 5.1), indicating that the differences in vertical transport of O<sub>3</sub>  
373 also contribute to lower JJA O<sub>3</sub> concentrations in China in the weakest monsoon

374 years than in the strongest monsoon years, but the impact of the differences in  
375 vertical transport is smaller than that of the differences in transboundary transport  
376 of O<sub>3</sub>.

### 377 **5.3 Impact of cross-tropopause transport on surface-layer O<sub>3</sub>** 378 **concentrations**

379 The cross-tropopause transport of O<sub>3</sub> from the stratosphere is an important  
380 source of tropospheric O<sub>3</sub>. Simulation O<sub>3</sub>\_ST is performed to quantify the impact  
381 of cross-tropopause transport on JJA surface-layer O<sub>3</sub> concentrations. The  
382 simulated JJA concentrations of O<sub>3</sub> in simulation O<sub>3</sub>\_ST (referred to as STO<sub>3</sub>) at  
383 the surface-layer averaged over 1986–2006 are presented in Fig. 7b. STO<sub>3</sub>  
384 shows maximum concentrations of 15–20 ppbv over northwestern China,  
385 contributing to the high O<sub>3</sub> concentrations in western China simulated in O3\_TOT.  
386 Averaged over China, the surface-layer concentration of JJA STO<sub>3</sub> is 8 ppbv,  
387 which is about 17% of that of JJA O<sub>3</sub> simulated in O3\_TOT. Concentrations of  
388 STO<sub>3</sub> increase with altitude; the ratio of STO<sub>3</sub> to O<sub>3</sub> simulated in O3\_TOT is about  
389 50% at 200 hPa and about 80% at 100 hPa. Figure 7e shows the differences in  
390 surface-layer STO<sub>3</sub> concentrations between the weakest and strongest monsoon  
391 years. Relative to the strongest monsoon years, surface-layer STO<sub>3</sub>  
392 concentrations are lower by 1–2 ppbv over central China and the Tibetan Plateau  
393 in the weakest monsoon years. Averaged over China, the difference in STO<sub>3</sub>  
394 between the weakest and strongest monsoon years is –0.45 ppbv, which only

395 accounts for 23% of the corresponding difference in  $\text{TOTO}_3$  and hence indicates  
396 that the variations in  $\text{O}_3$  transported from the stratosphere in different monsoon  
397 years are not the major factors that drive the interannual variations of JJA  
398 surface-layer  $\text{O}_3$  concentrations in China. Note that the cross-tropopause  $\text{O}_3$  flux  
399 in  $\text{O}_3_{\text{-TOT}}$  and  $\text{O}_3_{\text{-ST}}$  is specified with the synthetic ozone (“Synoz”) method  
400 (McLinden et al., 2000) with a constant cross-tropopause ozone flux of  $499 \text{ Tg O}_3$   
401  $\text{yr}^{-1}$ . The latest version of the GEOS-Chem model also has an option of using the  
402 linearized ozone (“Linoz”) parameterization scheme of McLinden et al. (2000) to  
403 represent  $\text{O}_3$  in the stratosphere, in which the ozone vertical profiles across the  
404 tropopause are relaxed back toward climatological profiles and hence  
405 cross-tropopause  $\text{O}_3$  flux varies with time step and location. We have tested using  
406 “Linoz” instead of “Synoz” and found that these two schemes obtain same  
407 conclusion about the impact of cross-tropopause  $\text{O}_3$  on JJA surface-layer  $\text{O}_3$  in  
408 China.

#### 409 **5.4 Impacts of the EASM on local chemical production of $\text{O}_3$**

410 The differences in  $\text{O}_3$  concentrations between  $\text{O}_3_{\text{-TOT}}$  and  $\text{O}_3_{\text{-TB}}$  simulations  
411 are attributed to the enhancement of  $\text{O}_3$  due to Chinese emissions, referred to as  
412 Chinese local  $\text{O}_3$  ( $\text{LOCO}_3$ ). Figure 7c shows that high concentrations of  $\text{LOCO}_3$   
413 are located in eastern China where the emissions of  $\text{O}_3$  precursors are large. The  
414 maximum  $\text{LOCO}_3$  concentrations reach 40–45 ppbv. The  $\text{LOCO}_3$  concentration  
415 averaged over the whole China is 18 ppbv, which is about 38% of the value

416 simulated in O3\_TOT. Figure 7f presents the differences in simulated LOCO<sub>3</sub>  
417 between the weakest and strongest EASM years. Relative to the strongest  
418 monsoon years, LOCO<sub>3</sub> concentrations in the weakest monsoon years are lower  
419 by 2–5 ppbv over southern China and slightly higher by up to 1 ppbv over central  
420 China. Averaged over China, the difference in LOCO<sub>3</sub> between the weakest and  
421 strongest monsoon years is -0.4 ppbv, which accounts for 20% of the  
422 corresponding difference in TOTO<sub>3</sub> and hence reflects the small impacts of  
423 monsoon strength on local chemical production of O<sub>3</sub>.

424 The small impacts of monsoon strength on local chemical production of O<sub>3</sub>  
425 can be further justified by examining the net chemical production of O<sub>3</sub> within the  
426 selected box (85°–120°E, 20°–46°N, the surface to 250hPa). Sum over the  
427 selected box, the net chemical production (chemical production – chemical loss)  
428 averaged over the weakest monsoon years is 39.0 Tg season<sup>-1</sup> in JJA, which is  
429 smaller than that averaged over the strongest monsoon years by 0.5%.

430

## 431 **6 Comparison of the impact of monsoon strength with the role of** 432 **changing emissions**

433 We perform simulations O<sub>3</sub>\_EMIS to compare the impact of changing monsoon  
434 strength (Section 4) with that of changing anthropogenic emissions on JJA O<sub>3</sub>  
435 concentrations. Two sensitivity simulations are conducted with 1986 and 2006  
436 anthropogenic emissions, respectively, and year 2006 meteorological parameters  
437 are used to drive both simulations. Relative to 1986, year 2006 emissions of NO<sub>x</sub>,

438 CO, and NMVOCs in China increase by 111%, 56%, and 9%, respectively,  
439 leading to increases in JJA surface-layer O<sub>3</sub> by 9–15 ppbv in southeastern China  
440 (Fig. 9). Note the locations of large increases in O<sub>3</sub> here are different from those of  
441 large differences in O<sub>3</sub> between the weakest and strongest monsoon years (Fig.  
442 4b). Averaged over China, the change in JJA surface-layer O<sub>3</sub> concentration  
443 owing to changes in emissions over 1986–2006 is +5.3 ppbv, which is larger than  
444 the difference in JJA surface-layer O<sub>3</sub> of 2.0 ppbv between the selected weakest  
445 and strongest monsoon years. However, the difference in surface-layer O<sub>3</sub>  
446 between the weak monsoon year 1998 and the strong monsoon year 1997 is –4.2  
447 ppbv, indicating that the impacts of the EASM on JJA O<sub>3</sub> can be particularly strong  
448 for certain years.

449

## 450 **7 Conclusions**

451 We examine the impacts of the East Asian summer monsoon (EASM) on  
452 interannual variations of summertime surface-layer O<sub>3</sub> concentrations over China  
453 using the GEOS-Chem model driven by the assimilated GEOS-4 meteorological  
454 data. The interannual variations of O<sub>3</sub> concentrations are quantified by values of  
455 mean absolute deviation (MAD) and absolute percent departure from the mean  
456 (APDM), based on the simulation of O<sub>3</sub> for years 1986–2006 with changes in  
457 meteorological parameters but fixed anthropogenic emissions at year 2005 levels.  
458 The MAD values of JJA surface-layer O<sub>3</sub> concentrations in China are in the range  
459 of 1.0–4.0 ppbv, with the largest values exceeding 2 ppbv found over  
460 northeastern China, coastal areas of South China, and the Tibetan Plateau. The

461 APDM values of JJA surface-layer O<sub>3</sub> concentrations are 2–5% over central  
462 eastern China, 1–3% in northwestern China, and 5–10% over the Tibetan Plateau  
463 as well as the border and coastal areas of South China.

464 With fixed anthropogenic emissions, simulated JJA O<sub>3</sub> concentrations  
465 averaged over China exhibit strong positive correlation (with a correlation  
466 coefficient of +0.75) with the East Asian summer monsoon index (EASMI) in the  
467 time period of 1986–2006, indicating that JJA O<sub>3</sub> concentrations are lower (or  
468 higher) in weaker (or stronger) EASM years. Relative to JJA surface-layer O<sub>3</sub>  
469 concentrations in the strongest EASM years (1990, 1994, 1997, 2002, and 2006),  
470 O<sub>3</sub> levels in the weakest EASM years (1988, 1989, 1996, 1998, and 2003) are  
471 lower over almost whole China with the national mean O<sub>3</sub> concentration lower by  
472 2.0 ppbv (or 4%).

473 Sensitivity studies are performed to identify the key processes through which  
474 the variations in EASM strength influence interannual variations of JJA O<sub>3</sub> in  
475 China. The difference in transboundary transport of O<sub>3</sub> is found to be the most  
476 dominant factor that leads to lower O<sub>3</sub> concentrations in the weakest EASM years  
477 than in the strongest EASM years. Relative to the strongest EASM years, the  
478 weakest EASM years have less inflow by 0.11 Tg season<sup>-1</sup> at the west boundary,  
479 larger inflow fluxes of O<sub>3</sub> by 4.2 Tg season<sup>-1</sup> at the south boundary and by 5.5 Tg  
480 season<sup>-1</sup> at the north boundary, and larger outflow by 12.9 Tg season<sup>-1</sup> at the east  
481 boundary, as horizontal mass fluxes of O<sub>3</sub> at the four lateral boundaries of the  
482 selected box (85°–120°E, 20°–46°N, the surface to 250 hPa) are calculated. As a

483 result, the weakest EASM years have larger outflow of O<sub>3</sub> than the strongest  
484 EASM years, which, together with the enhanced vertical convections in the  
485 weakest EASM years, explain about 80% of the differences in surface-layer O<sub>3</sub>  
486 concentrations between the weakest and strongest EASM years.

487 We also perform a sensitivity simulation O<sub>3</sub>\_EMIS to compare the impact of  
488 changing monsoon strength with that of changing anthropogenic emissions on  
489 JJA O<sub>3</sub> concentrations. Averaged over China, the change in JJA surface-layer O<sub>3</sub>  
490 concentration owing to changes in emissions over 1986–2006 is +5.3 ppbv, which  
491 is larger than the difference in JJA surface-layer O<sub>3</sub> of 2.0 ppbv between the  
492 selected weakest and strongest monsoon years. However, the difference in  
493 surface-layer O<sub>3</sub> between the weak monsoon year 1998 and the strong monsoon  
494 year 1997 is –4.2 ppbv, indicating that the impacts of the EASM on JJA O<sub>3</sub> can be  
495 particularly strong for certain years. Note that while the largest increases in O<sub>3</sub> by  
496 anthropogenic emissions are located over southeastern China, the largest  
497 impacts of EASM on O<sub>3</sub> are found over central and western China.

498

499 *Acknowledgements.* This work was supported by the National Basic Research  
500 Program of China (973 program, Grant 2014CB441202), the Strategic Priority  
501 Research Program of the Chinese Academy of Sciences Strategic Priority  
502 Research Program Grant No. XDA05100503, the National Natural Science  
503 Foundation of China under grant 41021004, as well as the China Meteorological

504 Administration special funding in atmospheric science GYHY200906020.

505

506 **References**

- 507 An, Z., Porter, S. C., Kutzbach, J. E., Wu, X., Wang, S., Liu, X., Li, X., Zhou, W.:  
508 Asynchronous Holocene optimum of the East Asian monsoon, *Quaternary*  
509 *Science Reviews*, 19, 743–762, doi:10.1016/S0277-3791(99)00031-1, 2000.
- 510 Bey, I., Jacob, D. J., Yantosca, Logan, R. M., J. A., Field, B. D., Fiore, A. M., Li, Q.,  
511 Liu, H. Y., Mickley, L. J., and Schultz, M. G.: Global modeling of tropospheric  
512 chemistry with assimilated meteorology: model description and evaluation, *J.*  
513 *Geophys. Res.*, 106, 23073–23095, doi:10.1029/2001JD000807, 2001.
- 514 Chan, L. Y., Liu, H. Y., Lam, K. S., Wang, T., Oltmans, S. J., and Harris, J. M.:  
515 Analysis of the seasonal behavior of tropospheric ozone at Hong Kong,  
516 *Atmos. Environ.*, 32, 159–168, doi:10.1016/S1352-2310(97)00320-8, 1998.
- 517 Chou, C. C. K., Liu, S. C., Lin, C. Y., Shiu, C. J., and Chang, K. H.: The trend of  
518 surface ozone in Taipei, Taiwan, and its causes: Implications for ozone  
519 control strategies, *Atmos. Environ.*, 40, 3898–3908,  
520 doi:10.1016/j.atmosenv.2006.02.018, 2006.
- 521 Cheung, V. T. F. and Wang, T.: Observational study of ozone pollution at a rural  
522 site in the Yangtze Delta of China, *Atmos. Environ.*, 35, 4947–4958,  
523 doi:10.1016/S1352-2310(01)00351-X, 2001.
- 524 Ding, A., and Wang, T.: Influence of stratosphere-to-troposphere exchange on the  
525 seasonal cycle of surface ozone at Mount Waliguan in western China,  
526 *Geophys. Res. Lett.*, 33, L03803, doi:10.1029/2005GL024760, 2006.
- 527 Ding, A. J., Wang, T., Thouret, V., Cammas, J.-P., and Nédélec, P.: Tropospheric  
528 ozone climatology over Beijing: analysis of aircraft data from the MOZAIC  
529 program, *Atmos. Chem. Phys.*, 8, 1-13, doi:10.5194/acp-8-1-2008, 2008.
- 530 Ding, Y. H. and Johnny, C. L. C.: The East Asian summer monsoon: an overview,  
531 *Meteorol. Atmos. Phys.*, 89, 117–142, doi:10.1007/s00703-005-0125-z, 2005.
- 532 Duan, J. C., Tan, J. H., Yang, L., Wu, S., and Hao, J. M.: Concentration, sources  
533 and ozone formation potential of volatile organic compounds (VOCs) during  
534 ozone episode in Beijing, *Atmos. Res.*, 88, 25–35,  
535 doi:10.1016/J.Atmosres.2007.09.004, 2008.
- 536 Fiore, A. M., Horowitz, L. W., Purves, D. W., Levy, H., Evans, M. J., Wang, Y., Li,  
537 Q., and Yantosca, R. M.: Evaluating the contribution of changes in isoprene  
538 emissions to 25 surface ozone trends over the eastern United States, *J.*  
539 *Geophys. Res.*, 110, D12303, doi:10.1029/2004JD005485, 2005.
- 540 Gao, J., Wang, T., Ding, A. J., and Liu, C. B.: Observational study of ozone and  
541 carbon monoxide at the summit of mount Tai (1534 m a.s.l.) in central-eastern  
542 China, *Atmos. Environ.*, 39, 4779–4791, doi:10.1016/j.atmosenv.2005.04.030,  
543 2005.
- 544 Gao, Y. X.: Some Problems on East-Asia Monsoon, Science Press, Beijing, 49–  
545 63, 1962 (in Chinese).

546 Guenther, A., Karl, T., Harley, P., Wiedinmyer, C., Palmer, P. I., and Geron, C.:  
547 Estimates of global terrestrial isoprene emissions using MEGAN (Model of  
548 Emissions of Gases Aerosols from Nature), *Atmos. Chem. Phys.*, 6, 3181–  
549 3210, doi:10.5194/acp-6-3181-2006, 2006.

550 Han, Z. W., Ueda, H., and Matsuda, K.: Model study of the impact of biogenic  
551 emission on regional ozone and the effectiveness of emission reduction  
552 scenarios over eastern China, *Tellus B*, 57, 12–27,  
553 doi:10.1111/j.1600-0889.2005.00132.x, 2005.

554 He, Y. J., Uno, I., Wang, Z. F., Pochanart, P., Li, J., and Akimoto, H.: Significant  
555 impact of the East Asia monsoon on ozone seasonal behavior in the boundary  
556 layer of Eastern China and the west Pacific region, *Atmos. Chem. Phys.*, 8,  
557 7543–7555, doi:10.5194/acp-8-7543-2008, 2008.

558 Huang, G.: An index measuring the interannual variation of the East Asian  
559 summer monsoon - The EAP index, *Adv. Atmos. Sci.*, 21, 41–52,  
560 doi:10.1007/Bf02915679, 2004.

561 Intergovernmental Panel on Climate Change (IPCC), *Climate change 2007: the*  
562 *physical science basis. Contribution of working group I to the fourth*  
563 *assessment report of the inter-governmental panel on climate change*, edited  
564 by: Solomon, S. et al., Cambridge University Press, Cambridge, United  
565 Kingdom and New York, 1–996, 2007.

566 Jeong, J. I., and Park, R. J.: Effects of the meteorological variability on regional air  
567 quality in East Asia, *Atmos. Environ.*, 69, 46–55,  
568 doi:10.1016/J.Atmosenv.2012.11.061, 2013.

569 Li, J. and Zeng, Q.: A unified monsoon index, *Geophys. Res. Lett.*, 29, 115-1–  
570 115-4, doi:10.1029/2001GL013874, 2002.

571 Li, J., Wang, Z., Akimoto, H., Gao, C., Pochanart, P., and Wang, X.: Modeling  
572 study of ozone seasonal cycle in lower troposphere over east Asia, *J.*  
573 *Geophys. Res.*, 112, D22S25, doi:10.1029/2006JD008209, 2007.

574 Lin, M., Holloway, T., Oki, T., Streets, D. G., and Richter, A.: Multi-scale model  
575 analysis of boundary layer ozone over East Asia, *Atmos. Chem. Phys.*, 9,  
576 3277–3301, doi:10.5194/acp-9-3277-2009, 2009.

577 Lin, W., Xu, X., Zhang, X., and Tang, J.: Contributions of pollutants from North  
578 China Plain to surface ozone at the Shangdianzi GAW Station, *Atmos. Chem.*  
579 *Phys.*, 8, 5889–5898, doi:10.5194/acp-8-5889-2008, 2008.

580 Liu, X., Chance, K., Sioris, C. E., Kurosu, T. P., Spurr, R. J. D., Martin, R. V., Fu, T.  
581 M., Logan, J. A., Jacob, D. J., Palmer, P. I., Newchurch, M. J., Megretskaia, I.  
582 A., and Chatfield, R. B.: First directly retrieved global distribution of  
583 tropospheric column ozone from GOME: comparison with the GEOS-CHEM  
584 model, *J. Geophys. Res.*, 111, D02308, doi:10.1029/2005JD006564, 2006.

585 Logan, J. A.: An analysis of ozonesonde data for the troposphere:  
586 Recommendations for testing 3-D models and development of a gridded

587 climatology for tropospheric ozone, *J. Geophys. Res.*, 104, 16115–16149,  
588 doi:10.1029/1998JD100096, 1999.

589 Lou, S. J., Liao, H., and Zhu, B.: Impacts of aerosols on surface-layer ozone  
590 concentrations in China through heterogeneous reactions and changes in  
591 photolysis rates, *Atmos. Environ.*, 85, 123–138,  
592 doi:10.1016/j.atmosenv.2013.12.004, 2014.

593 McLinden, C. A., Olsen, S. C., Hannegan, B., Wild, O., Prather, M. J., and Sundet,  
594 J.: Stratospheric ozone in 3-D models: A simple chemistry and the  
595 cross-tropopause flux, *J. Geophys. Res.*, 105, 14653–14665,  
596 doi:10.1029/2000JD900124, 2000.

597 Park, R. J., Jacob, D. J., Chin, M., and Martin, R. V.: Sources of carbonaceous  
598 aerosols over the United States and implications for natural visibility, *J.*  
599 *Geophys. Res.*, 108, 4355, doi:10.1029/2002JD003190, 2003.

600 Park, R. J., Jacob, D. J., Field, B. D., Yantosca, R. M., and Chin, M.: Natural and  
601 transboundary pollution influences on sulfate-nitrate-ammonium aerosols in  
602 the United States: Implications for policy, *J. Geophys. Res.*, 109, D15204,  
603 doi:10.1029/2003JD004473, 2004.

604 Piccot, S. D., Watson, J. J., and Jones, J. W.: A Global Inventory of Volatile  
605 Organic-Compound Emissions from Anthropogenic Sources, *J. Geophys.*  
606 *Res.*, 97, 9897–9912, doi:10.1029/92JD00682., 1992.

607 Pickering, K. E., Wang, Y. S., Tao, W. K., Price, C., and Muller, J. F.: Vertical  
608 distributions of lightning NO<sub>x</sub> for use in regional and global chemical transport  
609 models, *J. Geophys. Res.*, 103, 31203–31216, doi:10.1029/98JD02651,  
610 1998.

611 Pochanart, P., Akimoto, H., Kinjo, Y., and Tanimoto, H.: Surface ozone at four  
612 remote island sites and the preliminary assessment of the exceedances of its  
613 critical level in Japan, *Atmos. Environ.*, 36, 4235–4250,  
614 doi:10.1016/S1352-2310(02)00339-4, 2002.

615 Price, C., and Rind, D.: A Simple Lightning Parameterization for Calculating  
616 Global Lightning Distributions, *J. Geophys. Res.*, 97, 9919–9933,  
617 doi:10.1029/92JD00719, 1992.

618 Sander, S. P., Friedl, R. R., DeMore, W. B., Golden, D. M., Kurylo, M. J.,  
619 Hampson, R. F., Huie, R. E., Moortgat, G. K., Ravishankara, A. R., Kolb, C. E.,  
620 and Molina, M. J.: Chemical Kinetics and Photochemical Data for Use in  
621 Stratospheric Modeling, Technical Report JPL Publication 00-3, Jet  
622 Propulsion Laboratory, Pasadena, CA, 2000.

623 Seinfeld, J. H. and Pandis, S. N.: Atmospheric Chemistry and Physics, 2nd Edn.,  
624 John Wiley & Sons, Inc., Hoboken, New Jersey, 2006.

625 Shao, M., Tang, X. Y., Zhang, Y. H., and Li, W. J.: City clusters in China: air and  
626 surface water pollution, *Front. Ecol. Environ.*, 4, 353–361,  
627 doi:10.1890/1540-9295(2006)004[0353:CCICAA]2.0.CO;2, 2006.

628 Shindell, D., Kuylensstierna, J. C. I., Vignati, E., van Dingenen, R., Amann, M.,  
629 Klimont, Z., Anenberg, S. C., Muller, N., Janssens-Maenhout, G., Raes, F.,  
630 Schwartz, J., Faluvegi, G., Pozzoli, L., Kupiainen, K., Höglund-Isaksson, L.,  
631 Emberson, L., Streets, D., Ramanathan, V., Hicks, K., Oanh, N. T. K., Milly,  
632 G., Williams, M., Demkine, V., and Fowler, D.: Simultaneously mitigating  
633 near-term climate change and improving human health and food security,  
634 *Science*, 335, 183–189, doi: 10.1126/science.1210026, 2012.

635 Streets, D. G., Bond, T. C., Carmichael, G. R., Fernandes, S. D., Fu, Q., He, D.,  
636 Klimont, Z., Nelson, S. M., Tsai, N. Y., Wang, M., Woo, J. H. and Yarber, K. F.:  
637 An inventory of gaseous and primary aerosol emissions in Asia in the year  
638 2000, *J. Geophys. Res.*, 108, 8809, doi:10.1029/2002JD003093, 2003.

639 Takami, A., Wang, W., Tang, D. G., and Hatakeyama, S.: Measurements of gas  
640 and aerosol for two weeks in northern China during the winter-spring period of  
641 2000, 2001 and 2002, *Atmos. Res.*, 82, 688–697,  
642 doi:10.1016/J.Atmosres.2006.02.023, 2006.

643 Tanimoto, H., Sawa, Y., Matsueda, H., Uno, I., Ohara, T., Yamaji, K., Kurokawa,  
644 J., and Yonemura, S.: Significant latitudinal gradient in the surface ozone  
645 spring maximum over East Asia, *Geophys. Res. Lett.*, 32, L21805,  
646 doi:10.1029/2005GL023514, 2005.

647 Tang, J., Wen, Y. P., Xu, X. B., Zheng, X. D., Guo, S., and Zhao Y. C.: China  
648 Global Atmosphere Watch Baseline Observatory and its measurement  
649 program, in CAMS Annual Report 1994–95, pp. 56–65, China Meteorol. Press,  
650 Beijing, 1995.

651 Tao, S. and Chen, L.: A Review of Recent Research on the East Asia Summer  
652 Monsoon in China, *Monsoon Meteorology*, Oxford University Press, Oxford,  
653 United Kingdom, 60–92, 1987.

654 Tu, J., Xia, Z. G., Wang, H. S., and Li, W. Q.: Temporal variations in surface  
655 ozone and its precursors and meteorological effects at an urban site in China,  
656 *Atmos. Res.*, 85, 310–337, doi:10.1016/J.Atmosres.2007.02.003, 2007.

657 van der Werf, G. R., Randerson, J. T., Giglio, L., Collatz, G. J., Kasibhatla, P. S.,  
658 and Arellano Jr., A. F.: Interannual variability in global biomass burning  
659 emissions from 1997 to 2004, *Atmos. Chem. Phys.*, 6, 3423–3441,  
660 doi:10.5194/acp-6-3423-2006, 2006.

661 van Donkelaar, A., Martin, R. V., Leaitch, W. R., Macdonald, A. M., Walker, T. W.,  
662 Streets, D. G., Zhang, Q., Dunlea, E. J., Jimenez, J. L., Dibb, J. E., Huey, L.  
663 G., Weber, R., and Andreae, M. O.: Analysis of aircraft and satellite  
664 measurements from the Intercontinental Chemical Transport Experiment  
665 (INTEX-B) to quantify long-range transport of East Asian sulfur to Canada,  
666 *Atmos. Chem. Phys.*, 8, 2999–3014, doi:10.5194/acp-8-2999-2008, 2008.

667 Wang, B., and Ding, Q.: Global monsoon: Dominant mode of annual variation in  
668 the tropics, *Dynam. Atmos. Oceans*, 44, 165–183,

669 doi:10.1016/J.Dynatmoce.2007.05.002, 2008.

670 Wang, H. Q., Jacob, D. J., Le Sager, P., Streets, D. G., Park, R. J., Gilliland, A. B.,  
671 and van Donkelaar, A.: Surface ozone background in the United States:  
672 Canadian and Mexican pollution influences, *Atmos. Environ.*, 43, 1310–1319,  
673 doi:10.1016/j.atmosenv.2008.11.036, 2009.

674 Wang, H. X., Kiang, C. S., Tang, X. Y., Zhou, X. J., and Chameides, W. L.:  
675 Surface ozone: A likely threat to crops in Yangtze delta of China, *Atmos.*  
676 *Environ.*, 39, 3843–3850, doi:10.1016/j.atmosenv.2005.02.057, 2005.

677 Wang, T., Ding, A., Gao, J., and Wu, W. S.: Strong ozone production in urban  
678 plumes from Beijing, China, *Geophys. Res. Lett.*, 33, L21806,  
679 doi:10.1029/2006GL027689, 2006b.

680 Wang, T., Wong, H. L. A., Tang, J., Ding, A., Wu, W. S., and Zhang, X. C.: On the  
681 origin of surface ozone and reactive nitrogen observed at a remote mountain  
682 site in the northeastern Qinghai-Tibetan Plateau, western China, *J. Geophys.*  
683 *Res.*, 111, D08303, doi:10.1029/2005JD006527, 2006a.

684 Wang, T., Wei, X. L., Ding, A. J., Poon, C. N., Lam, K. S., Li, Y. S., Chan, L. Y.,  
685 and Anson, M.: Increasing surface ozone concentrations in the background  
686 atmosphere of Southern China, 1994–2007, *Atmos. Chem. Phys.*, 9, 6217–  
687 6227, doi:10.5194/acp-9-6217-2009, 2009.

688 Wang, Y., McElroy, M. B., Munger, J. W., Hao, J., Ma, H., Nielsen, C. P., and  
689 Chen, Y.: Variations of O<sub>3</sub> and CO in summertime at a rural site near Beijing,  
690 *Atmos. Chem. Phys.*, 8, 6355–6363, doi:10.5194/acp-8-6355-2008, 2008.

691 Wang, Y., Zhang, Y., Hao, J., and Luo, M.: Seasonal and spatial variability of  
692 surface ozone over China: contributions from background and domestic  
693 pollution, *Atmos. Chem. Phys.*, 11, 3511–3525,  
694 doi:10.5194/acp-11-3511-2011, 2011.

695 Wang, Z. F., Li, J., Wang, X. Q., Pochanart, P., and Akimoto, H.: Modeling of  
696 regional high ozone episode observed at two mountain sites (Mt. Tai and  
697 Huang) in East China, *J. Atmos. Chem.*, 55, 253–272,  
698 doi:10.1007/S10874-006-9038-6, 2006.

699 Webster, P. J., Magana, V. O., Palmer, T. N., Shukla, J., Tomas, R. A., Yanai, M.,  
700 and Yasunari, T.: Monsoons: Processes, predictability, and the prospects for  
701 prediction, *J. Geophys. Res.*, 103, 14451–14510, doi:10.1029/97JC02719,  
702 1998.

703 Wiedinmyer, C., Sakulyanontvittaya, T., and Guenther, A.: MEGAN FORTRAN  
704 Code V2.04 User Guide, available at:  
705 <http://acd.ucar.edu/~guenther/MEGAN/MEGAN.htm> (last access: 31 January  
706 2014), 2007.

707 Wild, O., and Akimoto, H.: Intercontinental transport of ozone and its precursors in  
708 a three-dimensional global CTM, *J. Geophys. Res.*, 106, 27729–27744,  
709 doi:10.1029/2000JD000123, 2001.

710 Wild, O., Zhu, X., and Prather, M. J.: Fast-j: Accurate simulation of in- and  
711 below-cloud photolysis in tropospheric chemical models, *J. Atmos. Chem.*, 37,  
712 245–282, doi:10.1023/A:1006415919030, 2000.

713 Wu, S. L., Mickley, L. J., Leibensperger, E. M., Jacob, D. J., Rind, D., and Streets,  
714 D. G.: Effects of 2000–2050 global change on ozone air quality in the United  
715 States, *J. Geophys. Res.*, 113, D06302, doi:10.1029/2007JD008917, 2008.

716 Xu, X., Lin, W., Wang, T., Yan, P., Tang, J., Meng, Z., and Wang, Y.: Long-term  
717 trend of surface ozone at a regional background station in eastern China  
718 1991–2006: enhanced variability, *Atmos. Chem. Phys.*, 8, 2595–2607,  
719 doi:10.5194/acp-8-2595-2008, 2008.

720 Yamaji, K., Ohara, T., Uno, I., Tanimoto, H., Kurokawa, J., and Akimoto, H.:  
721 Analysis of the seasonal variation of ozone in the boundary layer in East Asia  
722 using the Community Multi-scale Air Quality model: What controls surface  
723 ozone levels over Japan?, *Atmos. Environ.*, 40, 1856–1868,  
724 doi:10.1016/j.atmosenv.2005.10.067, 2006.

725 Yan, P., Li, X., Luo, C., Xu, X., Xiang, R., Ding, G., Tang, J., Wang, M., and Yu, X.:  
726 Observational Analysis of surface O<sub>3</sub>, NO<sub>x</sub>, and SO<sub>2</sub> in China, *Appl. Meteor.*,  
727 8, 53–61, 1997 (in Chinese).

728 Yan, P., Wang, M., Cheng, H., and Zhou, X. J.: Distributions and variations of  
729 surface ozone in Changshu, Yangtze Delta region, *Acta Metallurgica Sinica*,  
730 17, 205–217, 2003.

731 Yang, G., Fan, S., Tang, J., Jin, S., and Meng, Z.: Characteristic of surface ozone  
732 concentrations at Lin'an, *Res. Environ. Sci.*, 21, 31–35, 2008 (in Chinese).

733 Ye, D. Z.: Some Characteristics of the Summer Circulation over the  
734 Qinghai-Xizang (Tibet) Plateau and Its Neighborhood, *B. Am. Meteorol. Soc.*,  
735 62, 14–19, doi:10.1175/1520-0477(1981)062<0014:Scotsc>2.0.Co;2, 1981.

736 Yienger, J. J., and Levy, H.: Empirical-Model of Global Soil-Biogenic Nox  
737 Emissions, *J. Geophys. Res.*, 100, 11447–11464, doi:10.1029/95JD00370,  
738 1995.

739 Zhang, Y. H., Hu, M., Zhong, L. J., Wiedensohler, A., Liu, S. C., Andreae, M. O.,  
740 Wang, W., and Fan, S. J.: Regional Integrated Experiments on Air Quality  
741 over Pearl River Delta 2004 (PRIDE-PRD2004): Overview, *Atmos. Environ.*,  
742 42, 6157–6173, doi:10.1016/J.Atmosenv.2008.03.025, 2008.

743 Zhao, C., Wang, Y., Yang, Q., Fu, R., Cunnold, D., and Choi, Y.: Impact of East  
744 Asian summer monsoon on the air quality over China: View from space, *J.*  
745 *Geophys. Res.*, 115, D09301, doi:10.1029/2009JD012745, 2010.

746 Zhou, D., Ding, A., Mao, H., Fu, C., Wang, T., Chan, L. Y., Ding, K., Zhang, Y., Liu  
747 J., Lu, A. and Hao, N.: Impacts of the East Asian monsoon on lower  
748 tropospheric ozone over coastal South China, *Environ. Res. Lett.*, 8, 044011,  
749 doi:10.1088/1748-9326/8/4/044011, 2013.

750 Zhou, L. T. and Huang, R. H.: Interdecadal variability of summer rainfall in

751 Northwest China and its possible causes. *Int. J. Climatol.*, 30, 549–557.  
752 doi:10.1002/joc.1923, 2010.

753 Zhu, B., Akimoto, H., Wang, Z., Sudo, K., Tang, J., and Uno, I.: Why does surface  
754 ozone peak in summertime at Waliguan?, *Geophys Res Lett*, 31,  
755 doi:10.1029/2004gl020609, 2004.

756 Zhu, J., Liao, H., and Li, J.: Increases in aerosol concentrations over eastern  
757 China due to the decadal-scale weakening of the East Asian summer  
758 monsoon, *Geophys. Res. Lett.*, 39, L09809, doi:10.1029/2012GL051428,  
759 2012.

760

761

762

763 **Table 1.** The composite analyses of horizontal and vertical fluxes of O<sub>3</sub> (Tg  
764 season<sup>-1</sup>) for the selected box of (85°–120°E, 20°–46°N, the surface to 250 hPa)  
765 based on simulations O3\_TOT and O3\_TB. The values are averaged over the five  
766 weakest (1988, 1989, 1996, 1998, and 2003) and five strongest monsoon years  
767 (1990, 1994, 1997, 2002, and 2006), and the differences are calculated as  
768 (weakest-strongest). For horizontal fluxes, positive values indicate eastward or  
769 northward transport and negative values indicate westward or southward  
770 transport. For vertical fluxes, positive values indicate upward transport.

Side of the selected box	O3_TOT			O3_TB		
	Weakest	Strongest	Difference	Weakest	Strongest	Difference
Horizontal mass fluxes						
West	+83.7	+83.8	-0.1	+78.8	+78.9	-0.1
East	+106.5	+93.5	+12.9	+84.1	+73.1	+11.0
South	+13.4	+9.2	+4.2	+13.8	+10.5	+3.3
North	-19.3	-13.7	-5.5	-20.0	-15.0	-5.0
Vertical mass fluxes						
Top	+22.1	+20.7	+1.4	+16.5	+15.5	+1.0

771

772 **Figure Captions**

773

774 **Fig. 1.** (a) Simulated JJA surface-layer O<sub>3</sub> concentrations (ppbv) that are  
775 averaged over years 1986–2006 of simulation O3\_TOT. (b) Mean absolute  
776 deviation (MAD, ppbv) and (c) absolute percent departure from the mean  
777 (APDM, %) calculated with 1986–2006 simulation of O<sub>3</sub> in O3\_TOT.

778

779 **Fig. 2.** Comparisons of observed and simulated JJA mean surface-layer O<sub>3</sub>  
780 concentrations at Hok Tsui (22°13' N, 114°15' E) in Hong Kong (left) and Ryori  
781 (39°03'N, 144°82'E) in Japan (right). Correlation coefficient between simulations  
782 and observations is shown at top right corner of each panel, which is calculated  
783 over the time period with observations available.

784

785 **Fig. 3.** (a) The normalized time series of EASMI (blue bars, left y-axis) and the  
786 simulated JJA surface-layer O<sub>3</sub> concentrations (black line, right y-axis, ppbv)  
787 averaged over China for years of 1986–2006. (b) Spatial distribution of the  
788 correlation coefficients between the EASMI and the JJA surface-layer O<sub>3</sub>  
789 concentrations. The dotted areas indicate statistical significance with 95%  
790 confidence from a two-tailed Student's t-test. The EASMI are calculated using the  
791 GEOS-4 assimilated meteorological data.

792

793 **Fig. 4.** Horizontal distributions of (a) absolute and (b) percentage differences in  
794 JJA surface-layer O<sub>3</sub> concentrations between the five weakest and strongest  
795 EASM years (weakest–strongest). Pressure-longitude cross sections averaged  
796 over 20°–46°N for (c) absolute and (d) percentage differences in JJA O<sub>3</sub>  
797 concentrations between the five weakest and strongest EASM years (weakest–  
798 strongest). Results are from simulation O3\_TOT and unit is shown on top of each  
799 panel.

800

801 **Fig. 5.** The JJA mean horizontal winds at (a) 850 hPa and (b) 500 hPa averaged  
802 over 1986–2006. The composite differences in horizontal winds between the five  
803 weakest and strongest EASM years (weakest–strongest) at (c) 850 hPa and (d)  
804 500 hPa. Horizontal winds are from the GEOS-4 assimilated meteorological data.  
805 Unit is shown on top of each panel. The location of box (85°–120°E, 20°–46°N,  
806 the surface to 250 hPa) selected to capture the features of transboundary O<sub>3</sub>  
807 transport is also shown in (d).

808

809 **Fig. 6.** The composite differences in horizontal O<sub>3</sub> fluxes (shades, kg s<sup>-1</sup>) and  
810 winds (contours, m s<sup>-1</sup>) at (a) south, (b) north, (c) west, and (d) east boundaries of  
811 the selected box of (85°–120°E, 20°–46°N, the surface to 250 hPa) between the  
812 five weakest and strongest EASM years (weakest–strongest). Fluxes and winds

813 that are eastward or northward are positive, and those that are westward and  
814 southward are negative. Mass fluxes are from simulation O3\_TOT. Longitudinal  
815 and meridional winds are from the GEOS-4 assimilated meteorological data.

816

817 **Fig. 7.** The JJA surface-layer O<sub>3</sub> concentrations (ppbv) from (a) simulation  
818 O3\_TB (referred to as TBO<sub>3</sub>), (b) simulation O3\_ST (referred to as STO<sub>3</sub>), and (c)  
819 simulation O3\_TOT minus simulation O3\_TB (referred to as LOCO<sub>3</sub>). Panels (a),  
820 (b), and (c) are the averages over 1986–2006. Panels (d), (e), and (f) are the  
821 composite differences (ppbv) in TBO<sub>3</sub>, STO<sub>3</sub>, and LOCO<sub>3</sub>, respectively, between  
822 the five weakest and strongest EASM years (weakest–strongest).

823

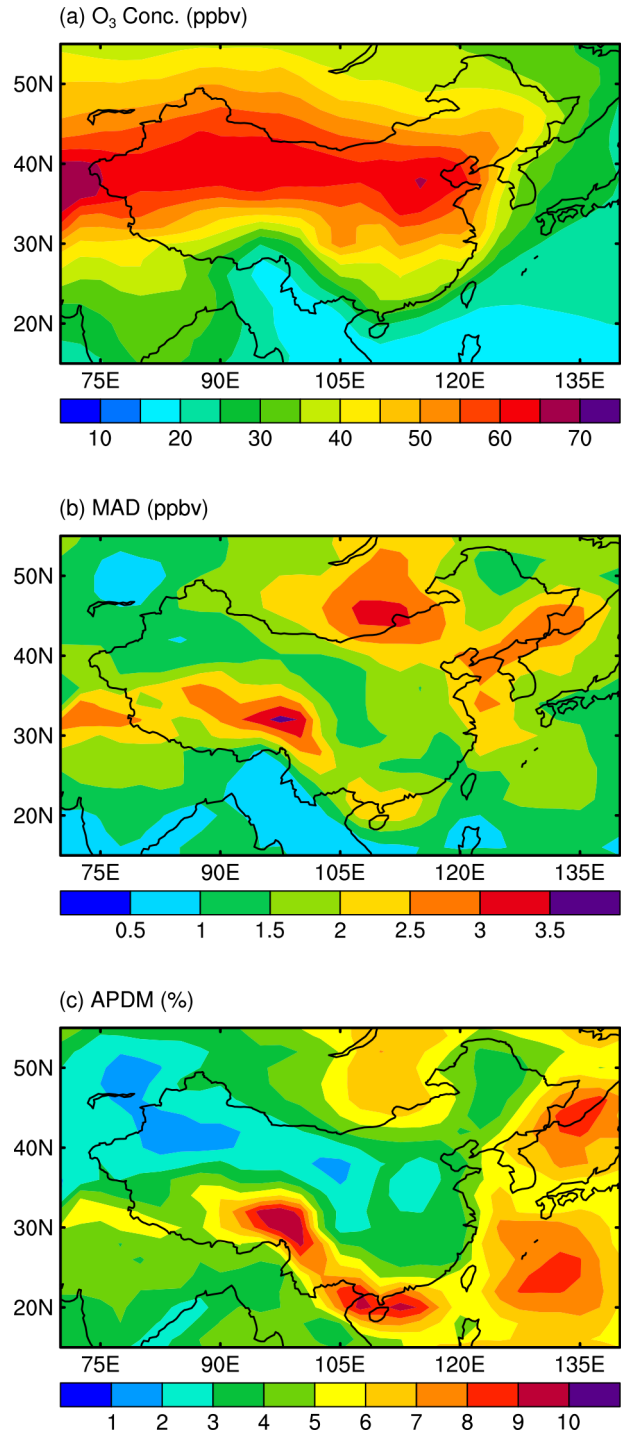
824 **Fig. 8.** (a) The spatial distributions of JJA mean vertical wind velocity (contours,  
825 Pa s<sup>-1</sup>\*1000) and simulated upward mass flux of O<sub>3</sub> (shades, kg s<sup>-1</sup>) averaged  
826 over 1986–2006. (b) The composite differences in vertical wind (contours, Pa  
827 s<sup>-1</sup>\*1000) and simulated upward mass flux of O<sub>3</sub> (shades, kg s<sup>-1</sup>) between the five  
828 weakest and strongest EASM years (weakest–strongest). Vertical winds are from  
829 the NCEP/NACR reanalysis data.

830

831 **Fig. 9.** The changes in simulated JJA surface-layer O<sub>3</sub> concentrations (ppbv)  
832 owing to the changes in anthropogenic emissions of O<sub>3</sub> precursors over 1986–  
833 2006, based on simulations of O3\_EMIS.

834

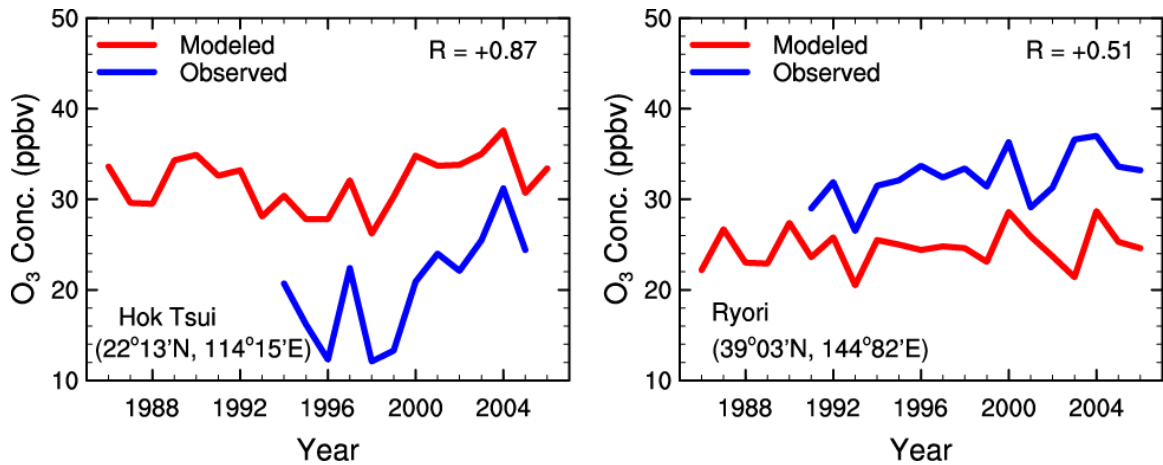
835



836

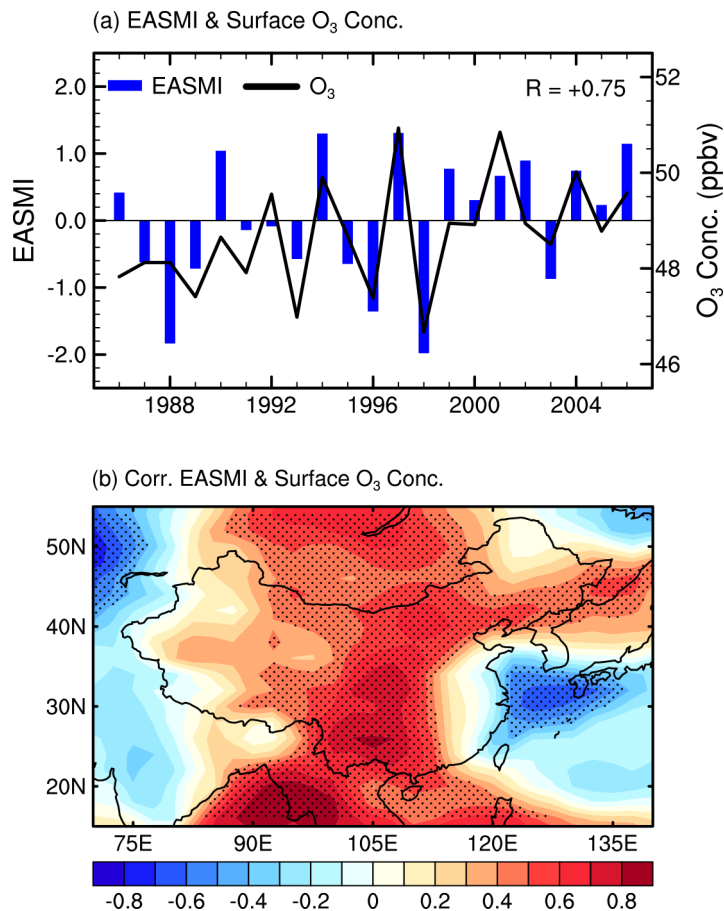
837

838 **Fig. 1.** (a) Simulated JJA surface-layer O<sub>3</sub> concentrations (ppbv) that are  
 839 averaged over years 1986–2006 of simulation O3\_TOT. (b) Mean absolute  
 840 deviation (MAD, ppbv) and (c) absolute percent departure from the mean  
 841 (APDM, %) calculated with 1986–2006 simulation of O<sub>3</sub> in O3\_TOT.



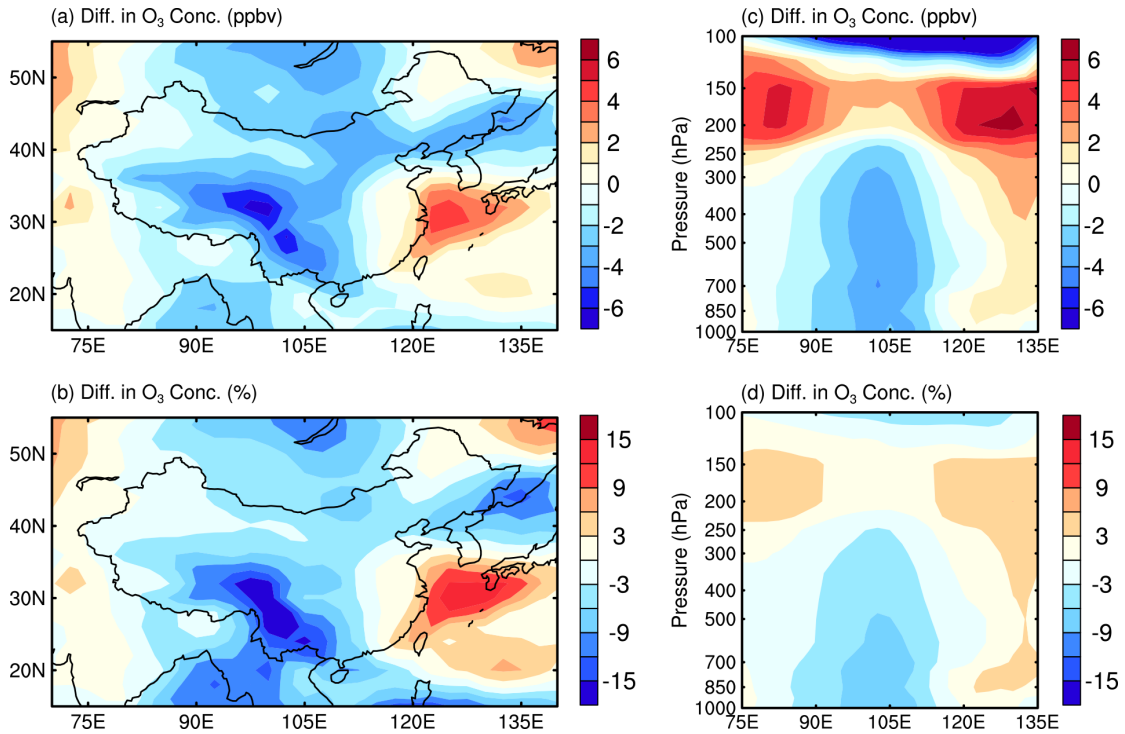
842  
 843  
 844  
 845  
 846  
 847  
 848  
 849

**Fig. 2.** Comparisons of observed and simulated JJA mean surface-layer O<sub>3</sub> concentrations at Hok Tsui (22°13' N, 114°15' E) in Hong Kong (left) and Ryori (39°03'N, 144°82'E) in Japan (right). Correlation coefficient between simulations and observations is shown at top right corner of each panel, which is calculated over the time period with observations available.



850  
 851  
 852  
 853  
 854  
 855  
 856  
 857  
 858  
 859

**Fig. 3.** (a) The normalized time series of EASMI (blue bars, left y-axis) and the simulated JJA surface-layer O<sub>3</sub> concentrations (black line, right y-axis, ppbv) averaged over China for years of 1986–2006. (b) Spatial distribution of the correlation coefficients between the EASMI and the JJA surface-layer O<sub>3</sub> concentrations. The dotted areas indicate statistical significance with 95% confidence from a two-tailed Student’s t-test. The EASMI are calculated using the GEOS-4 assimilated meteorological data.

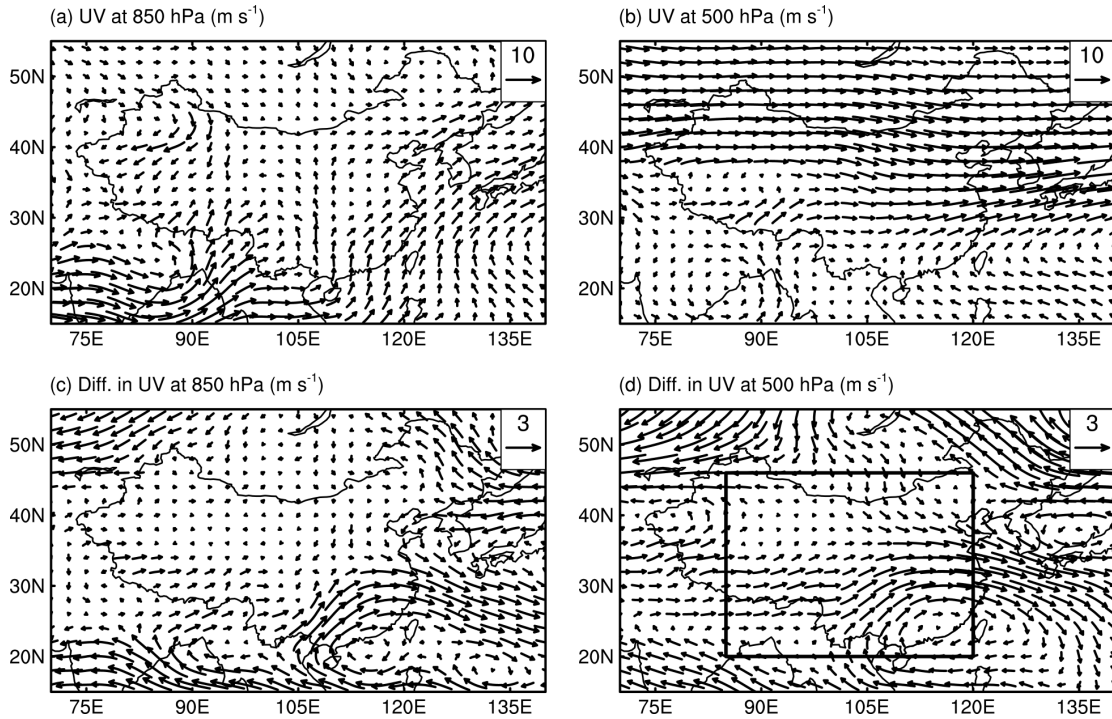


860

861

862 **Fig. 4.** Horizontal distributions of (a) absolute and (b) percentage differences in  
 863 JJA surface-layer O<sub>3</sub> concentrations between the five weakest and strongest  
 864 EASM years (weakest–strongest). Pressure-longitude cross sections averaged  
 865 over 20°–46°N for (c) absolute and (d) percentage differences in JJA O<sub>3</sub>  
 866 concentrations between the five weakest and strongest EASM years (weakest–  
 867 strongest). Results are from simulation O3\_TOT and unit is shown on top of each  
 868 panel.

869

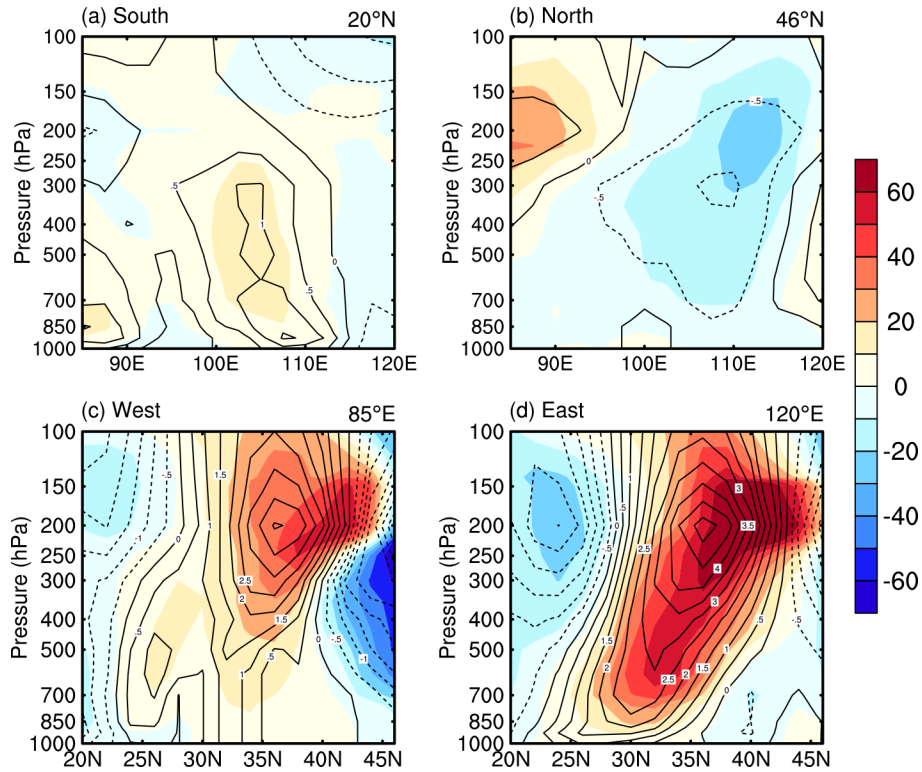


870

871

872 **Fig. 5.** The JJA mean horizontal winds at (a) 850 hPa and (b) 500 hPa averaged  
 873 over 1986–2006. The composite differences in horizontal winds between the five  
 874 weakest and strongest EASM years (weakest–strongest) at (c) 850 hPa and  
 875 500 hPa. Horizontal winds are from the GEOS-4 assimilated meteorological data.  
 876 Unit is shown on top of each panel. The location of box (85°–120°E, 20°–46°N,  
 877 the surface to 250 hPa) selected to capture the features of transboundary O<sub>3</sub>  
 878 transport is also shown in (d).

879

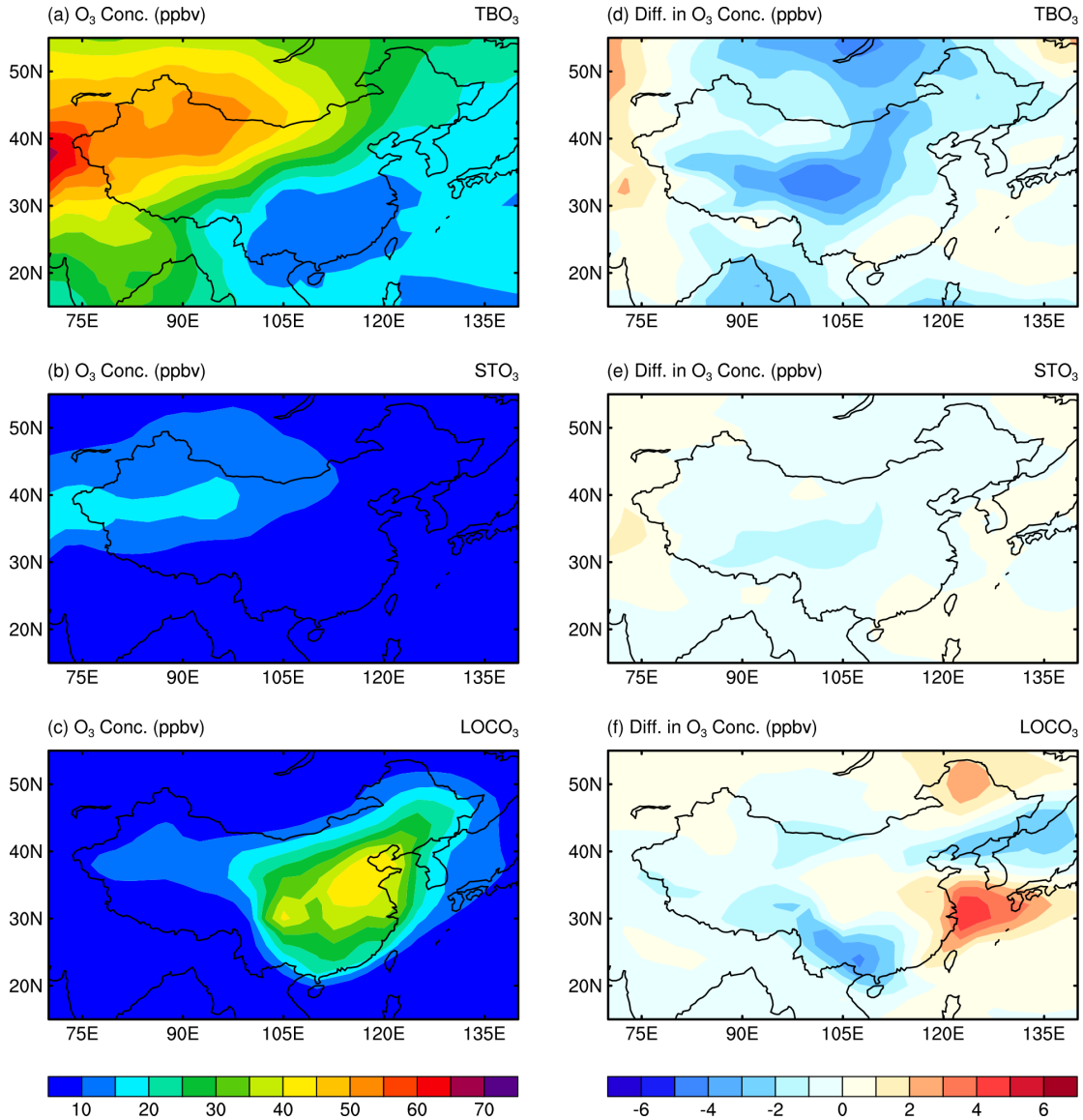


880

881

882 **Fig. 6.** The composite differences in horizontal O<sub>3</sub> fluxes (shades, kg s<sup>-1</sup>) and  
 883 winds (contours, m s<sup>-1</sup>) at (a) south, (b) north, (c) west, and (d) east boundaries of  
 884 the selected box of (85°–120°E, 20°–46°N, the surface to 250 hPa) between the  
 885 five weakest and strongest EASM years (weakest–strongest). Fluxes and winds  
 886 that are eastward or northward are positive, and those that are westward and  
 887 southward are negative. Mass fluxes are from simulation O3\_TOT. Longitudinal  
 888 and meridional winds are from the GEOS-4 assimilated meteorological data.

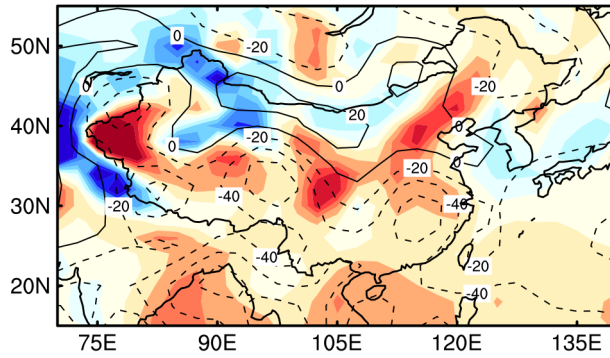
889



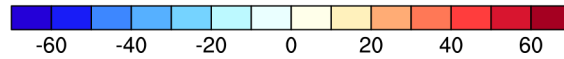
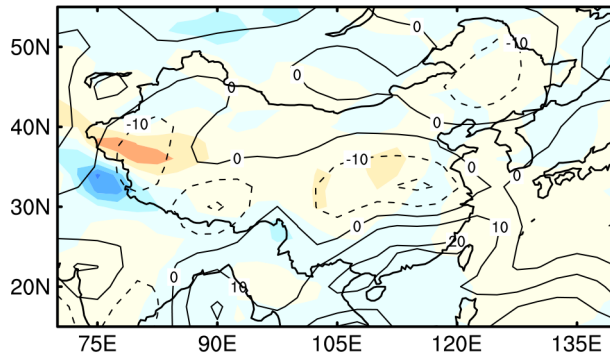
890  
891  
892  
893  
894  
895  
896  
897  
898  
899

**Fig. 7.** The JJA surface-layer O<sub>3</sub> concentrations (ppbv) from (a) simulation O3\_TB (referred to as TBO<sub>3</sub>), (b) simulation O3\_ST (referred to as STO<sub>3</sub>), and (c) simulation O3\_TOT minus simulation O3\_TB (referred to as LOCO<sub>3</sub>). Panels (a), (b), and (c) are the averages over 1986–2006. Panels (d), (e), and (f) are the composite differences (ppbv) in TBO<sub>3</sub>, STO<sub>3</sub>, and LOCO<sub>3</sub>, respectively, between the five weakest and strongest EASM years (weakest–strongest).

(a) OMEGA & O<sub>3</sub> vertical mass flux at 500 hPa

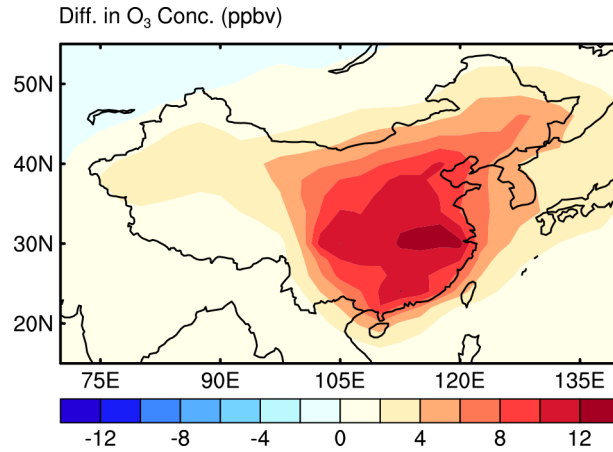


(b) Diff. in OMEGA & O<sub>3</sub> vertical mass flux at 500 hPa



900  
901  
902  
903  
904  
905  
906  
907  
908

**Fig. 8.** (a) The spatial distributions of JJA mean vertical wind velocity (contours, Pa s<sup>-1</sup>\*1000) and simulated upward mass flux of O<sub>3</sub> (shades, kg s<sup>-1</sup>) averaged over 1986–2006. (b) The composite differences in vertical wind (contours, Pa s<sup>-1</sup>\*1000) and simulated upward mass flux of O<sub>3</sub> (shades, kg s<sup>-1</sup>) between the five weakest and strongest EASM years (weakest–strongest). Vertical winds are from the NCEP/NACR reanalysis data.



909

910

911 **Fig. 9.** The changes in simulated JJA surface-layer O<sub>3</sub> concentrations (ppbv)  
912 owing to the changes in anthropogenic emissions of O<sub>3</sub> precursors over 1986–  
913 2006, based on simulations of O3\_EMIS.

914

915